Authors' accepted version of a paper published as
Quaternary Geochronology 42 (2017) 31-41.
http://dx.doi.org/10.1016/j.quageo.2017.07.006

Using thermoluminescence signals from feldspars for low-temperature thermochronology

N.D. Brown[a,*], E.J. Rhodes[a,b], T. Mark Harrison[a]

[a] *Department of Earth, Planetary, and Space Sciences, University of California, Los Angeles, 595 Charles Young Drive East, Box 951567, Los Angeles, CA 90095-1567, USA*
[b] *Department of Geography, Winter Street, University of Sheffield, Sheffield, South Yorkshire S10 2TN, UK*

Abstract

Natural thermoluminescence (TL) signals from feldspar crystals extracted from thermally stable drill cores ($T = -4.1 - 60.2$ °C) exhibit a strong dependence on geologic and laboratory thermal conditions. As burial temperature increases, the position of the TL glow curve at half-maximum intensity (i.e., the $T_{1/2}$ parameter) shifts to higher measurement temperatures. This shift is also observed following isothermal treatments in the laboratory. This relationship can be explained using a kinetic model originally developed for optical luminescence dating of feldspar grains. The thermal history of a sample is preserved in the degree of electron trap saturation as a function of thermal detrapping probability, which varies with recombination distance. A natural feldspar sample contains a range of thermal stabilities: the least stable traps will remain empty, the most stable will be full, and those traps which are partially filled will, in the case of thermal equilibrium, be diagnostic of the storage temperature. The $T_{1/2}$ parameter of a TL glow curve reflects which sites remain occupied. This interpretation is further borne out by additive dose measurements which illustrate that samples buried at lower temperatures are fully saturated at lower TL measurement temperatures ($\sim 200 - 300$ °C) relative to warmer samples. This signal is estimated to be useful in rapidly-cooling bedrock and should grow measurably for $\sim 10^2 - 10^6$ years.

Keywords: luminescence thermochronology, low-temperature thermochronology, feldspar thermoluminescence

1. Introduction

Luminescence signals from quartz and feldspar crystals extracted from bedrock samples have recently been shown to contain information useful for reconstructing geothermal histories (Herman

*Corresponding author
Email addresses: nathan.david.brown@ucla.edu (N.D. Brown), ed.rhodes@sheffield.ac.uk (E.J. Rhodes), tmark.harrison@gmail.com (T. Mark Harrison)

et al., 2010; Li and Li, 2012; Sarkar et al., 2013; Guralnik et al., 2013, 2015a,b; King et al., 2016b,c). The proposed effective closure temperatures for these signals extend below 100 °C, depending on the cooling rate and ambient temperature. Both quartz and feldspar luminescence signals face limitations, however, in their utility as thermochronometers. The fast component of optically stimulated luminescence (OSL) from bedrock quartz is characteristically dim, typically experiences dose saturation at lower doses than feldspar, and is commonly overprinted by brighter luminescence responses from inclusions, such as feldspar or zircon (Guralnik et al., 2015a). Whereas feldspar luminescence signals are brighter and saturate at higher doses than quartz, the non-first-order kinetics of detrapping (e.g., band-tail transitions, athermal fading via quantum mechanical tunneling) pose a significant challenge (Jain and Ankjaergaard, 2011; Jain et al., 2015). Luminescence signals of feldspar crystals extracted from crushed bedrock are the focus of this study.

As of yet, the only feldspar luminescence signals interrogated for thermochronometry have been the infrared stimulated luminescence (IRSL) signal from Na-feldspar, extracted from the thermally-stable KTB borehole in Germany (Guralnik et al., 2015b); the IRSL signal from surficial bedrock feldspars collected from a range of lithologies and exhumation rates (Valla et al., 2016); and IRSL signals at multiple elevated temperatures (MET) from Na- and K-rich feldspars within the rapidly-exhuming eastern Himalayan syntaxis (King et al., 2016b,c). Optically-stimulated luminescence techniques (including IRSL) offer several advantages for the luminescence dating of sediments in comparison to thermoluminescence (TL) signals: the measured signal bleaches more rapidly with sunlight exposure, and single grains can be individually stimulated with focused laser beams. However, for monitoring the dose response in a lightless but thermally-varying system, the TL signal may provide a distinct advantage. Specifically, the stimulating energy gradually increases during the measurement procedure, which produces luminescence from a continuum of thermal stabilities in a single glow curve (Strickertsson, 1985; Balescu et al., 1997). Unlike IRSL techniques, which stimulate with a constant optical power, TL is measured by gradually heating a sample from room temperature until the relevant traps are emptied (conventionally to a maximum of around 500 °C), and the luminescence emissions are monitored as a function of the temperature of the sample. Thermoluminescence emissions therefore reflect the range of occupied trap stabilities that have naturally accumulated. This study aims to characterize feldspar TL as a record of geothermal history.

Thermoluminescence has long been used to discern features about a sample's thermal history. Most often, researchers are interested in the time since the thermal-resetting of archaeological materials. Quartz is the more common target mineral in this context. Target materials include

fired ceramics (Aitken et al., 1964; Fleming et al., 1970), hearth stones (Plachy and Sutton, 1982), and burnt flint (Valladas and Valladas, 1987). A notable exception is the use of feldspar TL for the dating of burnt stones and ceramics (Mejdahl, 1983, 1985; Spencer and Sanderson, 1994, 2012).

When used for thermochronometry, thermoluminescence studies usually consider the decay of peaks in quartz crystals (e.g., Tang and Li, 2015). Prokein and Wagner (1994) observed the reduction of the quartz 325 °C TL peak over a wide range of steady-state temperatures (14 - 56 °C), and Nambu et al. (1996) made the more general observation of decreasing overall quartz TL intensity with burial temperature, an observation that was given more robust theoretical treatment in later work (Tsuchiya et al., 2000; Tsuchiya and Fujino, 2000; Schmidt et al., 2015). Gong et al. (2010) extended the ESR framework of Grün et al. (1999) to estimate apparent ages and paleotemperatures for the 375 and 425 °C TL peaks of quartz from sedimentary basins. Ypma and Hochman (1991) monitored the temperature shift of the bulk TL glow curve in quartz from sedimentary basins and noticed systematic shifts between basins with differential exhumation histories.

Thermoluminescence signals from lunar rocks and fines (e.g., plagioclase) have also been used to estimate the balance between irradiation and thermal depletion of traps. These studies produced quantitative estimates of sediment burial depth (Hoyt et al., 1970; Durrani et al., 1973), effective storage temperature (Durrani et al., 1972, 1973), thermal gradient (Hoyt et al., 1971), and even the duration of shadow cover for samples adjacent to boulders (Durrani et al., 1977). The present study extends that body of work by incorporating recent advances in the understanding of feldspar luminescence kinetics (e.g., detrapping by tunneling to nearby recombination centers; Jain et al., 2015) and by considering long-term storage of feldspars at upper-crustal temperatures in terrestrial drill cores.

This study examines both the natural and laboratory-induced TL signals from feldspar crystals extracted from split drill cores originally collected from Alaska, Colorado, and Wyoming that represent steady-state heat flows of 54.4, 58.3, and 100.4 mW/m^2, respectively. First, the TL signals of feldspars taken from different depths are measured. The natural signals are presented along with multiple-aliquot additive-dose (MAAD) and single-aliquot regenerative (SAR) dose responses, as well as isothermal decay measurements. Next, these signals are compared with results from a kinetic model similar to that of Jain et al. (2015) that assumes that: a) distance-dependent, excited-state tunneling is the primary pathway for feldspar luminescence; and b) that sites at increasing distances from centers will exhibit greater trapping stability. We simulate laboratory and natural isothermal conditions and compare the simulated results to our measurements. Finally, we suggest

future research directions.

2. Materials and methods

2.1. Geologic context and sample collection

A total of 20 samples were collected from split drill cores kept at the United States Geologic Survey Core Research Center (CRC), Lakewood, Colorado. The samples were chosen to represent a wide range of steady-state temperatures ($-4.1 - 60.2$ °C), within relatively uniform lithologies. The three cores sampled were from the North Slope of Alaska (CRC library code E802; $n = 5$; 69°50'18"N, 155°59'24"W), the Piceance Basin of northwestern Colorado (W219; $n = 8$; 39°53'36"N, 108°32'37"W), and the Greater Green River Basin of south-central Wyoming (R716; $n = 7$; 41°2'41"N, 108°6'39"W) (Fig. 1(a) and (b)).

Core E802 from the Colville Basin of North Slope Alaska is comprised of the Nanushuk Group: Lower and Upper Cretaceous sandstone, shale, and minor conglomerate deltaic wedge, all shed from the Brooks Range, a series of thrust sheets stacked during the Late Jurassic to Early Cretaceous arc-continent collision (Mull et al., 1987). Core W219 is comprised of the Green River Formation: Eocene interbedded mudstone and sandstone, carbonaceous shale, lenticular sandstones and thickly-bedded evaporites that were deposited in and around lacustrine basins formed during the Laramide orogeny (Irwin, 1977; Smith et al., 2008). Core R716 contains Eocene basin-fill (Wasatch Formation): floodplain deposits of lenticular of parallel-bedded sandstones, and mudstone (Roehler, 1992). Similar to W219, the R716 core was likely derived from Laramide basement (Fan et al., 2011).

To estimate the undisturbed modern subsurface temperatures for each core, the following steps were taken. For E802, the geothermal gradients above and below the ice-bearing permafrost layer were interpolated from nearby sites within the Colville Basin which were measured for a high-resolution temperature survey of wells considered to be in thermal equilibrium (Collett et al., 1993). For W219, a similar interpolation was performed using gradient-at-depth measurements from nearby sites within the Piceance Basin (Blackwell et al., 2011). For R716, a geothermal gradient map was used (Finn, 2005). From these geothermal gradient approximations, the modern temperature of each core sample was estimated (Fig. 1(b)). Further details about these measurements can be found in the Supplementary Materials.

Whether samples are in thermal equilibrium depends on the exhumation rate at each core site. The most rapid exhumation is at site W219. Although no measurements have been made at the core site itself, fluid inclusion microthermometry (Fall et al., 2012, 2015) and vitrine reflectance

data (Zhang et al., 2008) from the center of the Piceance Basin imply an exhumation rate of 0.16 - 0.24 km/Ma since 10 Ma, corresponding to a cooling rate of 3.8 °C/Ma within the Mesaverde Group (modern geothermal gradient of 53 °C/km), immediately below the Wasatch Formation (vitrine reflectance data suggest heat-flow values similar to modern since the Miocene). Moreover, the exhumation at the northern basin edge is expected to be slower than in the center (Zhang et al., 2008). Based on apatite fission track cooling ages, the exhumation rate for the Colville Basin (core E802) since the Paleocene has been about 0.05 - 0.06 km/Ma (Cole et al., 1997) and vitrine reflectance data suggest an exhumation rate of 0.01 - 0.02 km/Ma since the Eocene for the Green River Basin (core R716) (Jagniecki et al., 2013), both of which are effectively static for the TL signal considered here. The modern geothermal gradients at these sites are also much lower than at W219: 34 and 35 °C/km compared with 53 °C/km (see Supplementary Materials for more detail), which would result in cooling rates of 1.9 and 0.5 °C/Ma for E802 and R716, respectively. Because these cooling rates are considerably lower than the reported detectable cooling rates for other trapped-charge thermochronometric systems (e.g., >20 to 615 °C/Ma; Table 2 of King et al., 2016a), the modern undisturbed core temperature measurements are reported as 'steady-state' temperatures (T_{SS}) hereafter.

2.2. Sample preparation and instrumentation

To isolate the inner portion of the split drill cores, the samples were spray-painted and then the outer surfaces were removed using a rotary tool fitted with a tile-cutting bit. The unexposed inner portions from the drill core samples were then ground with a pestle and mortar and sieved to isolate the 175 - 400 μm size fraction. These separates were then treated with 3% hydrochloric acid and separated by density using lithium metatungstate heavy liquid ($\rho < 2.565$ g/cm^3; Rhodes 2015) in order to isolate the most potassic feldspar crystals. Crystals were mounted on stainless steel discs in a small-diameter (3 - 5 mm) monolayer using silicon oil.

The outer portions of each sample were analyzed with inductively-coupled plasma mass spectrometry (ICP-MS) to estimate the U and Th contents, and with inductively-coupled optical emission spectrometry (ICP-OES) to measure the K content. These values were converted into a geologic dose-rate using the factors of Adamiec and Aiken (1998). We estimate an internal dose-rate assuming a feldspar potassium content of 12.5 ± 0.5 wt% (Huntley and Baril, 1997). Beta attenuation is calculated assuming a water content of 0.5 ± 0.5%. The resulting geologic dose-rate values are listed in Table 1.

Table 1: Sample depths, steady-state temperatures, and dose-rate information.

Field code	Lab code	Depth (m)	T_{SS} (°C)	K (%)	Th (ppm)	U (ppm)	Total dose-rate (Gy/ka)
E802-1	J1012	159	-4.1	1.1	5.2	2.04	2.85 ± 0.11
E802-2	J1013	303	0.8	0.9	3.5	1.39	2.39 ± 0.10
E802-3	J1014	367	3.0	1.1	4.9	1.77	2.76 ± 0.11
E802-4	J1015	496	7.4	1.3	5.5	1.96	3.04 ± 0.12
E802-5	J1016	656	12.8	0.9	6.1	2.09	2.73 ± 0.10
W219-1	J1017	7	6.4	3.6	9.7	2.39	5.72 ± 0.27
W219-2	J1018	72	9.8	2.4	10.0	1.87	4.36 ± 0.19
W219-3	J1019	150	14.0	6.1	7.2	2.13	7.71 ± 0.43
W219-4	J1020	240	18.7	1.3	4.6	4.21	3.49 ± 0.13
W219-5	J1021*	321	23.0	1.6	3.5	2.34	3.27 ± 0.14
W219-6	J1022*	418	28.2	1.3	4.8	2.47	3.11 ± 0.12
W219-7	J1023*	509	33.0	2.2	12.1	3.55	4.70 ± 0.18
W219-8	J1024*	575	36.5	0.4	1.9	0.98	1.72 ± 0.08
R716-1	J1025	307	15.1	2.1	7.1	1.57	3.81 ± 0.17
R716-2	J1026	445	19.8	2.5	17.1	4.81	5.61 ± 0.21
R716-3	J1027	606	25.4	2.4	16.4	3.59	5.19 ± 0.20
R716-4	J1028	881	35.0	2.1	23.8	5.43	5.83 ± 0.21
R716-5	J1029	1030	40.1	1.9	13.8	2.82	4.36 ± 0.17
R716-6	J1030	1462	55.1	1.9	16.9	3.68	4.77 ± 0.18
R716-7	J1031	1609	60.2	0.9	3.2	2.15	2.60 ± 0.10

*The natural signals from these samples were conflated with black-body radiation emissions during measurement and are disregarded from further analysis.

Luminescence measurements were carried out at the UCLA luminescence laboratory using a TL-DA-20 Risø automated reader equipped with a $^{90}Sr/^{90}Y$ beta source. Thermoluminescence emissions were detected through a Schott BG3-BG39 filter combination (transmission window of 325 - 475 nm) in a nitrogen atmosphere.

3. Thermoluminescence signals from feldspars extracted from drill cores

3.1. Natural signals

Sixteen of the 20 measured samples produced natural TL signals suitable for analysis (Fig. 2). The four rejected samples were from core W219, were buried at temperatures ≥ 23 °C, and yielded natural signals dominated by black-body radiation (approximated by measuring TL from the same aliquot after the natural signal has been removed). This lack of natural signal likely results from the high burial temperatures experienced by these samples. In core R716, however, samples with higher T_{SS} values retained natural TL signals above black-body radiation levels. The natural variability in the upper limit of resolvable T_{SS} values deserves further exploration.

Because the low-temperature TL peak in feldspar is generally asymmetric with overlapping peaks at higher temperatures, it is common practice to describe natural TL curves according to the measurement temperature at half of the maximum TL intensity (i.e., the position of the 'leading edge' of the main peak in a TL glow curve), or $T_{1/2}$ (e.g., Spencer and Sanderson, 2012). As steady-state temperatures (T_{SS}) increase, the natural $T_{1/2}$ values shift to higher temperatures (Fig. 1c). Additionally, within a given core (each of which has a fairly uniform lithology), TL brightness tends to decrease at higher T_{SS} values (Fig. 2).

3.2. Field saturation

A primary concern when considering the dose-response characteristics of luminescence signals is a change in sensitivity during the course of a measurement sequence (Wintle and Huntley, 1982). To avoid any such changes in the dose-response sensitivity induced by heating, we tested the level of natural dose-saturation (i.e., 'field saturation'; Kars et al., 2008) in samples J1012 and J1030 by using a multiple-aliquot additive-dose (MAAD) approach. Separate aliquots were given beta doses in addition to their natural doses. The subsequent TL curves (Fig. 3a - b) show which regions of the glow curve are saturated (and do not, therefore, grow with dose) and which regions are not saturated (and grow with dose).

Sample J1012 is almost fully saturated from about 270 to 370 °C, with an average ratio of 0.95 ± 0.02. Sample J1030 shows a similar degree of saturation, 0.95 ± 0.03, from 340 to 410 °C (Fig. 3c). The key observation from this experiment is that T_{SS} relates to the TL measurement temperature at which traps are fully saturated (i.e., in field saturation; $T_{SS} = -4.1$ °C for J1012 and 55.1 °C for J1030). This indicates that burial temperature controls which regions within a TL curve are stable enough to accumulate charge over time. At higher measurement temperatures, both samples show

ratios greater than one, which may reflect the effect of dose-quenching (for a detailed description of this phenomenon in quartz, see Bailey, 2001) on a high-temperature peak (e.g., 410 °C TL peak; Murray et al., 2009). Why the samples are > 1 at different temperatures is unclear, but likely relates to the variability in the position of the high-temperature peak(s).

3.3. Signals following isothermal treatments

After the measurement of the natural signal, an aliquot of sample J1012 (core E802) was given a beta dose of 24 Gy and then subjected to a series of isothermal treatments: 50, 100, 150, and 200 °C for 10, 30, 100, 300, and 1000 s. Following these treatments, the TL signals were measured (Fig. 4). A shift to higher temperatures for the $T_{1/2}$ value and a reduction in TL intensity result from longer heat treatments and greater hold temperatures, an observation made previously (e.g., Spencer and Sanderson, 1994). This resembles the effect of burial at higher natural T_{SS} values (Fig. 2). Both of these effects are simulated later in this work in sections 4.3 and 4.4.

A higher temperature peak is evident, centered around 390 °C. High-temperature peaks (centered between $\sim$ 310 - 410 °C) are well-documented for feldspar TL studies and exhibit different luminescence properties than the lower-temperature peak and probably therefore involve a different combination of traps and/or recombination centers (Balescu et al., 1991; Duller, 1994, 1997; Murray et al., 2009). For that reason, our analysis is restricted to those regions unaffected by this higher-temperature peak.

4. A kinematic model of feldspar TL

4.1. Model description

In this study, we estimate the net change in the concentration of trapped electrons with the following expression

$$\frac{dn(r')}{dt} = \frac{\dot{D}}{D_0}\Big(N(r') - n(r')\Big) - n(r')\exp\Big(-\Delta E/k_B T\Big)\frac{P(r')s}{P(r')+s} \tag{1}$$

The accumulation term for every dimensionless recombination distance r' depends on the concentration of unoccupied traps ($N(r') - n(r')$), which will fill at a rate proportional to the dose-rate $\dot{D}$ (Gy/s), normalized by D_0, the dose (Gy) at which $(1 - e^{-1})$ of the total traps are filled (i.e., the characteristic dose) (Christodoulides et al., 1971). The total concentration of traps separated from a recombination center by some distance between r' and $r' + dr'$ is given by Huntley (2006) as

$$N(r')dr' = N \cdot 3(r')^2 \exp\big(-(r')^3\big)dr' \tag{2}$$

Table 2: Parameter values used in kinetic model.

Parameter	Description	Value
$\dot{D}$	Dose rate	4 Gy·ka^{-1} (geologic) or 0.1 Gy·s^{-1} (laboratory)
D_0	Characteristic dose	1.6 kGy
ΔE	Activation energy to excited state	1.3 eV
P_0, s	Frequency factors	2×10^{16} s^{-1}
ρ'	Dimensionless recombination center density	1.32×10^{-3}

The loss term multiplies the concentration of trapped electrons at some distance $n(r')$ by their recombination probability. Following recent work (Jain et al., 2015; Pagonis et al., 2016), we approximate the detrapping probability in feldspar as localized transitions to randomly-distributed luminescence centers. This probability is governed by the activation energy from the ground- to the excited-state, ΔE (eV), the temperature of the lattice, T (K), the attempt-to-escape frequency factor, s (s^{-1}), and the excited-state tunneling probability, $P(r')$ (s^{-1}). The tunneling probability decreases with r' according to the relationship

$$P(r') = P_0 \exp(-\rho'^{-1/3} r') \tag{3}$$

where P_0 (s^{-1}) is the attempt-to-tunnel probability and ρ' the dimensionless concentration of recombination centers in the lattice (Huntley, 2006). A more complete model description is found in the Supplementary Materials.

By numerically solving Equation 1 for geothermal or laboratory conditions, we can evaluate how the trapped electron population, $n(r')$, evolves through time (all simulations presented in this work were evaluated with the ode23tb solver within MATLAB). The resulting $n(r')$ array can then be taken as the input for a simulated TL measurement. The expression for TL intensity as a function of measurement time is given as

$$I_{TL}(t) \propto \int_{t=0}^{t_F} \int_{r'=0}^{\infty} n(r') dr' dt \tag{4}$$

when a sample is heated from $T = 0$ to T_F at $dT/dt = \beta$ °C/s. The final measurement time, t_F, is the final temperature, T_F, divided by the heating rate, β.

4.2. Model parameter values

The behavior of Eq. 1 is sensitive to the parameter values chosen. In this section, we describe the values used in this study. While all of the values presented here are consistent with available

literature values and with experimental results, it should be stressed that many of these values will vary between samples. The careful quantification of these parameters will be a prerequisite for the quantification of thermal histories using feldspar TL signals.

4.2.1. Geologic ($\dot{D}_G$) and laboratory ($\dot{D}_L$) dose rates

The average environmental dose rate for all samples is 4.0 ± 1.5 Gy/ka, represented by our chosen $\dot{D}_G$ value of 4 Gy/ka. The laboratory dose rate, $\dot{D}_L$, administered by the ^{90}Sr/^{90}Y beta source at UCLA has been measured to be 0.1 Gy/s at the sample location using the standard calibration quartz sample supplied from Risø DTU National Laboratory. This value is used to simulate laboratory irradiations.

4.2.2. Characteristic dose, D_0

The TL dose response of sample J1012 is shown in Fig 5(a) following single-aliquot regenerative doses ranging from 0 to 3.9 kGy. Because we are concerned with growth in the region of the TL curve near the natural $T_{1/2}$ values, we examine the saturation behavior around the 230 °C region of the glow curves ($T_{1/2}$ = 223, 223, 227, and 236 °C for J1012; purple TL curves in Fig. 2). Specifically, we fit the TL values to a single saturating exponential function of the form

$$I = I_{max}(1 - \exp^{-D/D_0}) \tag{5}$$

where I is the TL intensity which increases with given dose D up to some maximum intensity I_{max} (Christodoulides et al., 1971). In this region, we see an average D_0 value of 1.6 kGy. Such a value is consistent with previous additive dose observations (e.g., Balescu and Lamothe, 1992; Balescu et al., 1997).

Given the multiple-aliquot additive-dose (MAAD) results reported in the Section 3.2, it appears as though the TL intensity at the natural $T_{1/2}$ value derives from those traps which will remain only partially filled ($n/N < 0.86$) at the relevant geologic dose-rate and temperature. In this view, a conservative approach would be to examine the dose-responses at more stable portions of the curve to avoid measuring traps that would fill at laboratory but not geologic dose-rates. We therefore report a D_0 value of 1.6 kGy, a value taken from the range $260 < T\ (^\circ\mathrm{C}) < 270$.

Ultimately, this parameter will control the time required for a sample to equilibrate to thermal steady-state and should therefore be quantified thoroughly when addressing transient responses to thermal perturbation. For our study, where sites have been cooling very slowly for at least 10 Ma ($t >> 2D_0/\dot{D}$), this parameter will not significantly affect our drill core fitting results. In

rapidly-cooling bedrock, however, this term will influence the length of time that traps will remain in disequilibrium.

4.2.3. Frequency factors, P_0 and s

For the attempt-to-tunnel and attempt-to-escape frequency factors (P_0 and s, respectively) we use a reasonable but arbitrary value of 2×10^{16} s^{-1}. Post-isothermal TL analyses (Brown and Rhodes, 2017) of J1012 suggest that the effective frequency factors involved in TL production, i.e., $\big(P(r')s\big)/\big(P(r')+s\big)$ term within Equation 1, range from 10^{14} to 10^{18} s^{-1}, decreasing monotonically as a function of isothermal holding temperature or duration.

Despite the fact that the P_0 and s values have different physical meanings (pp. 48-49, McKeever, 1985; Tsuchiya et al., 1987) and may vary by orders of magnitude (Jain et al., 2015), we assign them the same numerical value for goodness-of-fit and simplicity (we express both terms individually in Equation 1).

4.2.4. Activation energy, ΔE, and recombination center density, ρ'

Jain et al. (2015) introduced the following expression to describe isothermal TL from feldspars:

$$L \propto -\frac{dn}{dt} = 3n_0\rho' z(t')^{-1}\bigg(\ln(t'P_0) - \xi\bigg)^2 \exp\bigg(-\rho'\bigg(\ln(t'P_0) - \xi\bigg)^3\bigg) \tag{6}$$

where $t' = \tau_0 + zt$ and $\xi = \Delta E/k_B T$, with n_0 representing the concentration of trapped electrons at the start of the measurement and z representing the rate of change for the lifetime of trapped charge (following Huntley (2006) and Jain et al. (2012), we set $z = 1.8$). The variable τ_0 represents the critical lifetime at the start of the measurement. Both n_0 and τ_0 depend upon the radiation history of a sample and are best-fit parameters. Assuming that recombination proceeds by tunneling from the excited state to randomly-distributed luminescence centers, isothermal TL at any hold temperature should approximately follow Eq. 6.

Fig. 5(b) shows the isothermal decay of an aliquot of J1012 held at 250, 300, and 350 °C for 1000 s (400 s of which is shown). These data are fitted with Eq. 6 using the same parameters used in the main text to fit the $T_{1/2}$ values for all drill core samples at natural and laboratory conditions, namely: $\Delta E = 1.3$ eV, $\rho' = 1.32 \times 10^{-3}$ and $P_0 = 2 \times 10^{16}$ s^{-1}.

4.3. Simulated TL responses following isothermal geologic histories

Using Eq. 1 and the parameter values listed in Table 2 (with the average geologic dose rate $\dot{D}_G$ for all samples of 4 Gy/ka), we modelled the evolution of $n(r')$ for hold temperatures of 0,

10, and 20 °C, and durations of 20 ka, 200 ka, and 2 Ma. After 800 ka ($2D_0/\dot{D}_G$), assuming the parameters listed in Table 2, the most stable traps (highest r' values) will be effectively saturated, i.e., $n/N \sim 0.86$ (see also Fig. 7). After 2 Ma, these traps should be entirely full ($n/N \sim 1$). The final distribution of $n(r')$ after each treatment was then evaluated using Eq. 4 to produce a synthetic TL curve; these are shown in Fig. 6a.

Two features are remarkable. First, and most relevant for this study, the TL peaks are emitted at higher stimulation temperatures when trapping occurs at higher temperatures. This is because those sites which are nearer to centers (i.e., have lower r' values) are unstable at higher ambient temperatures, and are therefore empty during the natural TL measurement. Second, the integrated emissions are greater for those simulations at lower temperatures. The reason for this is that the ratio of excited-to-ground-state electrons (n_e/n_g) depends exponentially on temperature ($n_e/n_g = \exp(-\Delta E/k_B T)$) and this ratio controls the rate of detrapping (see the Supplementary Materials for more detail).

4.4. Simulated TL responses following isothermal treatments

The same approach was used to predict the effects of short duration heat treatments. For each of these simulations, laboratory irradiation was reproduced by changing the dose rate, $\dot{D}$, to 0.1 Gy/s (this mimics the dose-rate received by crystals exposed to the ^{90}Sr/^{90}Y beta source at UCLA) and allowing the $n(r')$ distribution to evolve for 200 s (a simulated laboratory dose of 20 Gy) at 20 °C. Next, this $n(r')$ distribution was used as the initial condition of an isothermal heat treatment. The simulated hold times were 100, 300, and 1000 s; and the temperatures were 100, 150, and 200 °C. Finally, the $n(r')$ distribution was evaluated with Eq. 4, producing the TL curves shown in Fig. 6c.

The effects of heating are to shift the TL emissions to higher measurement temperatures and to reduce the peak intensity. This reason for this behavior is the progressive thermal erosion of those sites which have lower recombination distances; the more stable sites comprise the higher temperature regions of the TL measurements.

4.5. Trapping at a single recombination distance

Equation (1) can also be used to illustrate the evolution of trap populations under different scenarios. An arbitrary recombination distance of r' (e.g., 1.5) and a constant temperature of −4.1 °C (e.g., sample J1012) are examined within a 2 Ma simulation (Fig. 7a). The results are shown as the fraction of traps which are filled (when $n/N = 1$, all available traps are filled). Once

about 86% of traps are filled, even small variations in the measured luminescence response will lead to large or infinite errors in age determination and the trap is effectively saturated (Wintle and Murray, 2006). This saturation level is described with the D_0 parameter (effective saturation occurring at doses $> \ 2D_0$). In our case, we prescribe a value of $D_0 = 1.6$ kGy based on dose response measurements of sample J1012 (Fig. 5a); higher values result in a greater time required to reach saturation.

In our simulation, trap filling through time progresses as expected for a discrete trap (Fig. 7a). As the available sites fill, the fractional saturation behaves as a saturating exponential function. Notice that at the chosen temperature, this site will not fill entirely ($n/N < 1$). In other words, a thermal steady-state ($(n/N)_{SS}$) is reached which is incompletely saturated (cf. Christodoulides et al., 1971). Of course, with randomly distributed luminescence centers many recombination distances will occur, as discussed in the following section.

4.6. Trapping at all recombination distances

Considering all recombination distances present in the lattice and assuming randomly distributed centers, we can visualize trapping as a function of both time and recombination distance. Using Eq. 1, trapping is simulated at $T = -4.1$°C for durations of 0.25, 0.5, 1, and 2 Ma (Fig. 7b). The results shown in Fig. 7a are indicated with the light blue line for reference. Those traps with centers nearer than about $r' = 1.7$ will not saturate completely (given the prescribed temperature and dose rate) and sites at $r' \lesssim 0.8$ will not accumulate a significant concentration of electrons. Such sites would accumulate appreciable charge, however, if the temperature were lowered sufficiently. Nevertheless, after 2 Ma all sites are in thermal steady-state ($(n/N)_{SS}$) and their concentrations will not change until the temperature changes.

4.7. Trapping at drill core temperatures

Finally, the simulation conducted in Section 4.6 is repeated for the steady-state temperatures experienced by drill core samples J1012, J1026, and J1030 (T_{SS} = -4.1, 19.8, and 55.1 °C, respectively) (Fig. 7c). The r' values greater than about 1.48 reach effective saturation ($n/N > 0.86$) after some amount of time (in this example, sites nearer to centers than $r' = 1.48$ experience thermally-assisted tunneling at a rate higher than the filling rate). The more stable sites saturate after 800 ka, but some of the less stable sites reach saturation later. This is because the detrapping rate is greater for these sites.

Higher mean temperatures result in a trapped population with greater minimum r' values. In other words, the nearer sites that would be occupied at lower temperatures remain empty at higher temperatures. This trend in site occupancy with temperature can be examined in the measured TL signals from drill core samples, which is discussed in the following section.

5. Comparing measured and modeled behaviors

5.1. Comparing natural signals to modeled signals

The $T_{1/2}$ values for all drill core natural TL signals are shown as open symbols in Fig. 6b. Also shown as a solid black curve in Fig. 6b are the $T_{1/2}$ values simulated at natural conditions. To produce these values, we first solve Eq. 1 for the time range $t = 0$ to 2 Ma at each sample's burial temperature, T_{SS}. The resulting $n(r')$ distribution for each sample is evaluated with Eq. 4 to determine the TL that would result after burial at T_{SS} for 2 Ma. A remarkable correlation is found, suggesting that the measured relationship between natural $T_{1/2}$ values and the steady-state temperature is explainable in terms of site stability.

5.2. Comparing isothermal decay of TL signals to modeled response

The $T_{1/2}$ values following laboratory irradiation and heat treatment are plotted as open symbols in Fig. 6d. Also plotted are the $T_{1/2}$ values that are simulated with Eqs. 1 and 4, given the same kinetic parameters used in Fig. 6b. It is encouraging that the same kinetic parameters that reproduce the natural drill core $T_{1/2}$ values also resemble the high-temperature measurements.

This correlation between measured and simulated $T_{1/2}$ values gets stronger at longer durations and higher temperatures, which may suggest that our model fails to incorporate transient luminescence phenomena occurring at room temperature. Ground-state tunneling is omitted from the current model, but this effect should only decrease the minimum stability distance, shifting the $T_{1/2}$ value higher. This discrepancy deserves further consideration.

6. Discussion and Conclusions

Thermoluminescence signals from bedrock feldspars show a systematic dependence on ambient temperature. During burial, the electron traps within these crystals were filled according to the stability of each trapping site. Because this stability should depend on the distance to the nearest recombination center, a distribution of trap saturation as a function of distance develops, $n(r')$, which characterizes a samples thermal history. In the case of thermal steady-state, some sites

are entirely filled ($n/N \sim 1$), some are partially filled, and some remain empty (Fig. 7b). This partially-occupied recombination distance controls the position of the $T_{1/2}$ measurements shown for the natural signals and for signals following isothermal treatments (Figs. 6b and d).

The systematic dependence of natural $T_{1/2}$ values on ambient temperature (Fig. 6b) coupled with the multiple-additive dose results (Fig. 3) imply that T_{SS} controls trapping site occupancy and therefore the natural shape of feldspar TL, a behavior that can be explained in light of recent advances in our understanding of feldspar luminescence kinetics (e.g., Jain et al., 2015; Pagonis et al., 2016). Within this context, the role of anomalous fading should be considered. In our formulation (Eq. 1), fading is incorporated, though only in the excited-state (i.e., thermally-assisted tunneling). Thermally-activated tunneling can produce the phenomenon of anomalous fading as commonly measured in sediment studies (e.g., a decrease in luminescence intensity after storage at room temperature; Huntley and Lamothe, 2001), though with current parameter values, the magnitude of simulated room temperature fading is much lower than is experimentally observed. The observed fading rate will depend primarily upon the activation energy required to access the excited state, the ambient temperature, the effective frequency factor, and the density of recombination centers.

Of particular note is the agreement that we observe between model predictions and measured TL responses following natural and high-temperature laboratory heating conditions (Fig. 6). The same kinetic parameters (Table 2) described in Section 4.2 can be evaluated with Eq. 1 to reproduce the $T_{1/2}$ position resulting from 1000 s at 200 °C ($T_{1/2}$ offset by 15 °C; Fig. 6d) and thermal steady-state ($t \gtrsim$ order 10^5 ka) at -4.1 °C ($T_{1/2}$ offset by 5 °C; Fig. 6b).

We emphasize that this model is one of the simplest justifiable models for feldspar luminescence. Additional pathways that could be incorporated in the future might include activation into the band-tail states (up to the conduction band) or ground-state tunneling, both of which have been adopted for IRSL thermochronometry with feldspars (e.g., Guralnik et al., 2015b; King et al., 2016b). The main elements of this kinetic model are identical to those used in Jain et al. (2015) and have been used in that and other studies (Kitis and Pagonis, 2013; Pagonis et al., 2016) to explain both optical and thermal features of feldspar luminescence. Thermoluminescence signals may be preferable over optical luminescence for feldspar thermochronology applications, however, as the full range of thermal stability is monitored during a single TL measurement. Additionally, TL measurements avoid the complications arising from preheating and phototransfer effects.

Moving forward, many questions remain to fully develop this method. Does the feldspar TL response become more sensitive to radiation with prolonged heating or metamorphism? Both the TL

shape change after heating to 500 °C (Brown, 2017) and the observation that the degree of felspar ordering correlates with the degree of fading (p. 189, Aitken, 1985; Visocekas et al., 1994) suggest that peak metamorphic conditions may influence the subsequent rate of charge accumulation. What is the maximum steady-state temperature that can be identified using the leading edge of TL emissions? In core W219, the natural TL signals were too low to resolve the $T_{1/2}$ value at $T \geq 23.0$ °C, whereas for core R716, all samples gave useful TL signals, up to the highest temperatures measured: 60.2 °C. How should one handle low-temperature shoulders when identifying the natural $T_{1/2}$ value? It may be useful to separate shoulders by curve deconvolution, for example. Can we analytically define the closure temperature for a TL age resulting from different geothermal scenarios, or can this only be defined numerically? What is the natural variation for the parameters of Table 2? Efforts are underway currently to explore this variation for both optical and thermal signals in feldspars (Sfampa et al., 2015; Guralnik et al., 2015b; Valla et al., 2016; Brown and Rhodes, 2017). Is excited-state tunneling to randomly-distributed luminescence centers the primary detrapping pathway at geologic conditions? For example, initial simulations of linear cooling scenarios (not shown here) indicate that the TL system presented here may remain in thermal disequilibrium at cooling rates as slow as about 10 °C/Ma, but this result depends strongly on the parameter values chosen as well as the incorporated recombination pathways.

Our results illustrate the potential utility of the feldspar TL signal for geothermal studies. The $n(r')$ distribution is sensitive to a wide range of ambient temperatures: $-4.1 - 60.2$ °C. This distribution responds to thermally dynamic scenarios as well and initial simulations suggest that the signal should be useful for monitoring rapid exhumation during the Quaternary. This combination of low-temperature sensitivity and measurable signal growth between 10^2 to 10^6 years is promising for tectonic and geomorphic applications involving short-wavelength, upper-crustal thermal perturbations, and could prove useful in resolving questions of recent bedrock exhumation rates.

Acknowledgements

We thank Pierre Valla and Benny Guralnik for their insightful comments which have significantly improved this work. We also thank the USGS Core Research Center for providing drill core subsamples for analysis.

References

Adamiec, G., Aiken, M., 1998. Dose-rate conversion factors: update. Ancient TL 16, 37–50.

Aitken, M., 1985. Thermoluminescence Dating. Academic Press, London.

Aitken, M., Tite, M., Reid, J., 1964. Thermoluminescent dating of ancient ceramics. Nature 202, 1032–1033.

Bailey, R., 2001. Towards a general kinetic model for optically and thermally stimulated luminescence of quartz. Radiation Measurements 33, 17–45.

Balescu, S., Lamothe, M., 1992. The blue emission of K-feldspar coarse grains and its potential for overcoming TL age underestimation. Quaternary Science Reviews 11, 45–51.

Balescu, S., Lamothe, M., Lautridou, J.P., 1997. Luminescence evidence for two Middle Pleistocene interglacial events at Tourville, northwestern France. Boreas 26, 61–72.

Balescu, S., Packman, S.C., Wintle, A.G., 1991. Chronological separation of interglacial raised beaches from northwestern Europe using thermoluminescence. Quaternary Research 35, 95–102.

Blackwell, D., Richards, M., Frone, Z., Batir, J., Ruzo, A., Dingwall, R., Williams, M., 2011. Temperature at depth maps for the conterminous US and geothermal resource estimates. Geothermal Resources Council Transactions 35, 1545–1550.

Brown, N.D., 2017. Using luminescence signals from bedrock feldspars for low-temperature thermochronology. Ph.D. thesis. University of California, Los Angeles.

Brown, N.D., Rhodes, E.J., 2017. Thermoluminescence measurments of trap depth in alkali feldspars extracted from bedrock samples. Radiation Measurements 96, 53–61.

Christodoulides, C., Ettinger, K.V., Fremlin, J.H., 1971. The use of TL glow peaks at equilibrium in the examination of the thermal and radiation history of minerals. Modern Geology 2, 275–280.

Cole, F., Bird, K.J., Toro, J., Roure, F., O'Sullivan, P.B., Pawlewicz, M., Howell, D.G., 1997. An integrated model for the tectonic development of the frontal Brooks Range and Colville Basin 250 km west of the Trans-Alaska Crustal Transect. Journal of Geophysical Research 102, 20685–20708.

Collett, T., Bird, K., Magoon, L., 1993. Subsurface temperatures and geothermal gradients on the North Slope of Alaska. Cold Regions Science and Technology 21, 275–293.

Duller, G., 1997. Behavioural studies of stimulated luminescence from feldspars. Radiation Measurements 27, 663–694.

Duller, G.A.T., 1994. A new method for the analysis of infrared stimulated luminescence data from potassium feldspars. Radiation Measurements 23, 281–285.

Durrani, S., Prachyabrued, W., Christodoulides, C., Fremlin, J., 1972. Thermoluminescence of Apollo 12 samples: Implications for lunar temperature and radiation histories. Proceedings of the Third Lunar Science Conference 3, 2955–2970.

Durrani, S., Prachyabrued, W., Hwang, F., Edgington, J., Blair, I., 1973. Thermoluminescence of Apollo 14 and 16 fines and rock samples. Thermoluminescence of some Apollo 14 and 16 fines and rock samples 3, 2465–2479.

Durrani, S.A., Khazal, K.A.R., Ali, A., 1977. Temperature and duration of the shadow of a recently-arrived lunar boulder. Nature 266, 411–415.

Fall, A., Eichhubl, P., Bodnar, R.J., Laubach, S.E., Davis, J.S., 2015. Natural hydraulic fracturing of tight-gas sandstone reservoirs, Piceance Basin, Colorado. GSA Bulletin 127, 61–75.

Fall, A., Eichhubl, P., Cumella, S.P., Bodnar, R.J., Laubach, S.E., Becker, S.P., 2012. Testing the basin-centered gas accumulation model using fluid inclusion observations: Southern Piceance Basin, Colorado. AAPG Bulletin 96, 2297–2318.

Fan, M., Quade, J., Dettman, D., DeCelles, P., 2011. Widespread basement erosion during the late Paleocene-early Eocene in the Laramide Rocky Mountains inferred from $^{87}Sr/^{86}Sr$ ratios of freshwater bivalve fossils. GSA Bulletin 123, 2069–2082.

Finn, T.M., 2005. Petroleum systems and geologic assessment of oil and gas in the Southwestern Wyoming Province, Wyoming, Colorado, and Utah. U.S. Geological Survey. chapter Geothermal gradient map of the Southwestern Wyoming Province, southwestern Wyoming, northwestern Colorado, and northeastern Utah.

Fleming, S., Moss, H., Joseph, A., 1970. Thermoluminescence authenticity testing of some 'six dynasty' figurines. Archaeometry 12, 57–63.

Gong, G.L., Li, S.H., Sun, W.D., Guo, F., Xia, B., Lu, B.F., 2010. Quartz thermoluminescence - another potential paleo-thermometer for studies of sedimentary basin thermal history. Chinese Journal of Geophysics 53, 103–112.

Grün, R., Tani, A., Gurbanov, A., Koschug, D., Williams, I., Braun, J., 1999. A new method for the estimation of cooling and denudation rates using paramagnetic centers in quartz: A case study on the Eldzhurtinskiy Granite, Caucasus. Journal of Geophysical Research 104, 17531–17549.

Guralnik, B., Ankjaergaard, C., Jain, M., Murray, A., Muller, A., Walle, M., Lowick, S., Preusser, F., Rhodes, E., Wu, T.S., Mathew, G., Herman, F., 2015a. OSL-thermochronometry using bedrock quartz: A note of caution. Quaternary Geochronology 25, 37 – 48.

Guralnik, B., Jain, M., Herman, F., Ankjaergaard, C., Murray, A.S., Valla, P.G., Preusser, F., King, G.E., Chen, R., Lowick, S.E., Kook, M., Rhodes, E.J., 2015b. OSL-thermochronometry of feldspar from the KTB borehole, Germany. Earth and Planetary Science Letters 423, 232 – 243.

Guralnik, B., Jain, M., Herman, F., Paris, R.B., Harrison, T.M., Murray, A.S., Valla, P.G., Rhodes, E.J., 2013. Effective closure temperature in leaky and/or saturating thermochronometers. Earth and Planetary Science Letters 384, 209–218.

Herman, F., Rhodes, E.J., Braun, J., Heiniger, L., 2010. Uniform erosion rates and relief amplitude during glacial cycles in the Southern Alps of New Zealand, as revealed from OSL-thermochronology. Earth and Planetary Science Letters 297, 183–189.

Hoyt, H., Miyajima, M., Walker, R., Zimmerman, D., Zimmerman, J., 1971. Radiation dose rates and thermal gradients in the lunar regolith: Thermoluminescence and DTA of Apollo 12 samples. Proceedings of the Second Lunar Science Conference 3, 2245–2263.

Hoyt, H.P., Kardos, J.L., Miyajima, M., Seitz, M.G., Sun, S.S., Walker, R.M., Wittels, M.C., 1970. Thermoluminescence, X-ray and stored energy measurements of Apollo 11 samples. Proceedings of the Apollo 11 Lunar Science Conference 3, 2269–2287.

Huntley, D., Baril, M., 1997. The K content of the K-feldspars being measured in optical dating or in thermoluminescence dating. Ancient TL 15, 11–13.

Huntley, D.J., 2006. An explanation of the power-law decay of luminescence. Journal of Physics: Condensed Matter 18, 1359–1365.

Huntley, D.J., Lamothe, M., 2001. Ubiquity of anomalous fading in K-feldspars and the measurement and correction for it in optical dating. Canadian Journal of Earth Sciences 38, 1093–1106.

Irwin, D., 1977. Subsurface cross-sections of Colorado. Rocky Mountain Association of Geologists.

478 Jagniecki, E.A., Jenkins, D.M., Lowenstein, T.K., Carroll, A.R., 2013. Expermental study of shortite
479 ($Na_2Ca_2(CO_3)_3$) formation and application to the burial history of the Wilkins Peak Member,
480 Green River Basin, Wyoming, USA. Geochemica et Cosmochimica Acta 115, 31–45.

481 Jain, M., Ankjaergaard, C., 2011. Towards a non-fading signal in feldspar: Insight into charge
482 transport and tunnelling from time-resolved optically stimulated luminescence. Radiation Mea-
483 surements 46, 292–309.

484 Jain, M., Guralnik, B., Andersen, M.T., 2012. Stimulated luminescence emission from localized
485 recombination in randomly distributed defects. Journal of Physics: Condensed Matter 24, 385402.

486 Jain, M., Sohbati, R., Guralnik, B., Murray, A., Kook, M., Lapp, T., Prasad, A., Thomsen, K.,
487 Buylaert, J., 2015. Kinetics of infrared stimulated luminescence from feldspars. Radiation Mea-
488 surements 81, 242–250.

489 Kars, R., Wallinga, J., Cohen, K., 2008. A new approach towards anomalous fading correction for
490 feldspar IRSL dating–tests on samples in field saturation. Radiation Measurements 43, 786–790.

491 King, G., Guralnik, B., Valla, P.G., Herman, F., 2016a. Trapped-charge thermochronometry and
492 thermometry: A status review. Chemical Geology 446, 3–17.

493 King, G., Herman, F., Lambert, R., Valla, P., Guralnik, B., 2016b. Multi-OSL-thermochronometry
494 of feldspar. Quaternary Geochronology 33, 76–87.

495 King, G.E., Herman, F., Guralnik, B., 2016c. Northward migration of the eastern himalayan
496 syntaxis revealed by OSL thermochronometry. Science 353, 800–504.

497 Kitis, G., Pagonis, V., 2013. Analytical solutions for stimulated luminescence emission from tun-
498 neling recombination in random distributions of defects. Journal of Luminescence 137, 109–115.

499 Li, B., Li, S.H., 2012. Determining the cooling age using luminescence-thermochronology. Tectono-
500 physics 580, 242–248.

501 McKeever, S.W.S., 1985. Thermoluminescence of solids. Cambridge University Press, Cambridge.

502 Mejdahl, V., 1983. Feldspar inclusion dating of ceramics and burnt stones, in: Third Specialist
503 Seminar on TL and ESR Dating.

504 Mejdahl, V., 1985. Thermoluminescence dating based on feldspars. Nuclear Tracks and Radiation
505 Measurments 10, 133–136.

506 Mull, C., Roeder, D., Tailleur, I., Pessel, G., Grantz, A., May, S., 1987. Geologic sections and maps
507 across Brooks Range and Artic Slope to Beaufort Sea, Alaska. Geological Society of America.

508 Murray, A., Buylaert, J., Thomsen, K., Jain, M., 2009. The effect of preheating on the IRSL signal
509 from feldspar. Radiation Measurements 44, 554–559.

510 Nambu, M., Mikami, K., Tsuchiya, N., Nakatsuka, K., 1996. Thermoluminescence of quartz in
511 the borehole cores from the Minase Geothermal area, Akita Prefecture, Japan. Journal of the
512 Geothermal Research Society of Japan 18, 39–49.

513 Pagonis, V., Ankjaergaard, C., Jain, M., Chithambo, M.L., 2016. Quantitative analysis of time-
514 resolved infrared stimulated luminescence in feldspars. Physica B 497, 78–85.

515 Plachy, A., Sutton, S., 1982. Determination of the dose-rate to quartz in granite, in: PACT, AATA.
516 pp. 188–194.

517 Prokein, J., Wagner, G., 1994. Analysis of thermoluminescent glow peaks in quartz derived from
518 the KTB-drill hole. Radiation Measurements 23, 85–94.

519 Rhodes, E., 2015. Dating sediments using potassium feldspar single-grain IRSL: initial methodolog-
520 ical considerations. Quaternary International 362, 14–22.

521 Roehler, H.W., 1992. Correlation, composition, areal distribution, and thickness of Eocene strati-
522 graphic units, Greater Green River Basin, Wyoming, Utah, and Colorado. Geology of the
523 Eocene Wasatch, Green River, and Bridger (Washakie) Formations, Greater Green River Basin,
524 Wyoming, Utah, and Colorado, U.S. Geological Survey.

525 Sarkar, S.D., Mathew, G., Pande, K., Chauhan, N., Singhvi, A., 2013. Rapid denudation of higher
526 Himalaya during Late Pliestocene, evidence from OSL thermochronology. Geochronometria 40,
527 304–310.

528 Schmidt, C., Friedrich, J., Zöller, L., 2015. Thermochronometry using red TL of quartz? Numerical
529 simulation and observations from in-situ drill-hole samples. Radiation Measurements 81, 98–103.

530 Sfampa, I., Polymeris, G., Pagonis, V., Theodosoglou, E., Tsirliganis, N., Kitis, G., 2015. Correla-
531 tion of basic TL, OSL and IRSL properties of ten K-feldspar samples of various origins. Nuclear
532 Instruments and Methods in Physics Research B 359, 89–98.

Smith, M., Carroll, A., Singer, B., 2008. Synoptic reconstruction of a major ancient lake system: Eocene Green River Formation, western United States. GSA Bulletin 120, 54–84.

Spencer, J.Q., Sanderson, D.C.W., 1994. Mapping thermal exposure by luminescence thermometry. Radiation Measurements 23, 465–468.

Spencer, J.Q.G., Sanderson, D.C.W., 2012. Decline in firing technology or poorer fuel resources? high-temperature thermoluminscence (httl) archaeothermometry of neolithic ceramics from pool, sanday, orkney. Journal of Archaeological Science 39, 3542–3552.

Strickertsson, K., 1985. The thermoluminescence of potassium feldspars–glow curve characteristics and initial rise measurements. Nuclear Tracks and Radiation Measurements 10, 613–617.

Tang, S.L., Li, S.H., 2015. Low temperature thermochronology using thermoluminescence signals from quartz. Radiation Measurements 81, 92–97.

Tsuchiya, M., Atsusue, T., Sakaki, H., 1987. Tunneling escape rate of electrons from quantum well in double-barrier heterostructures. Physical Review Letters 59, 2356–2359.

Tsuchiya, N., Fujino, K., 2000. Evaluation of cooling history of the Quaternary Takidani pluton using thermoluminescence technique, in: Proceedings of the World Geothermal Congress, pp. 3939–3944.

Tsuchiya, N., Suzuki, T., Nakatsuka, K., 2000. Thermoluminescence as a new research tool for the evaluation of geothermal activity of the Kakkonda geothermal system, northeast Japan. Geothermics 29, 27–50.

Valla, P.G., Lowick, S.E., Herman, F., Champagnac, J.D., Steer, P., Guralnik, B., 2016. Exploring $IRSL_{50}$ fading variability in bedrock feldspars and implications for OSL thermochronometry. Quaternary Geochronology 36, 55–66.

Valladas, H., Valladas, G., 1987. Thermoluminescence dating of burnt flint and quartz: Comparative results. Archaeometry 29, 214–220.

Visocekas, R., Spooner, N., Zink, A., Blanc, P., 1994. Tunnel afterglow, fading and infrared emission in thermoluminescence of feldspars. Radiation Measurements 23, 377–385.

Wintle, A., Huntley, D., 1982. Thermoluminescence dating of sediments. Quaternary Science Reviews 1, 31–53.

Wintle, A., Murray, A., 2006. A review of quartz optically stimulated luminescence characteristics and their relevance in single-aliquot regeneration dating protocols. Radiation Measurements 41, 369–391.

Ypma, P., Hochman, M., 1991. Thermoluminescence geothermometry - a case study of the Otway Basin. The Australian Petroleum Exploration Association Journal 35, 312–324.

Zhang, E., Hill, R.J., Katz, B.J., Tang, Y., 2008. Modeling of gas generation from the Cameo coal zone in the Piceance Basin, Colorado. AAPG Bulletin 92, 1077–1106.

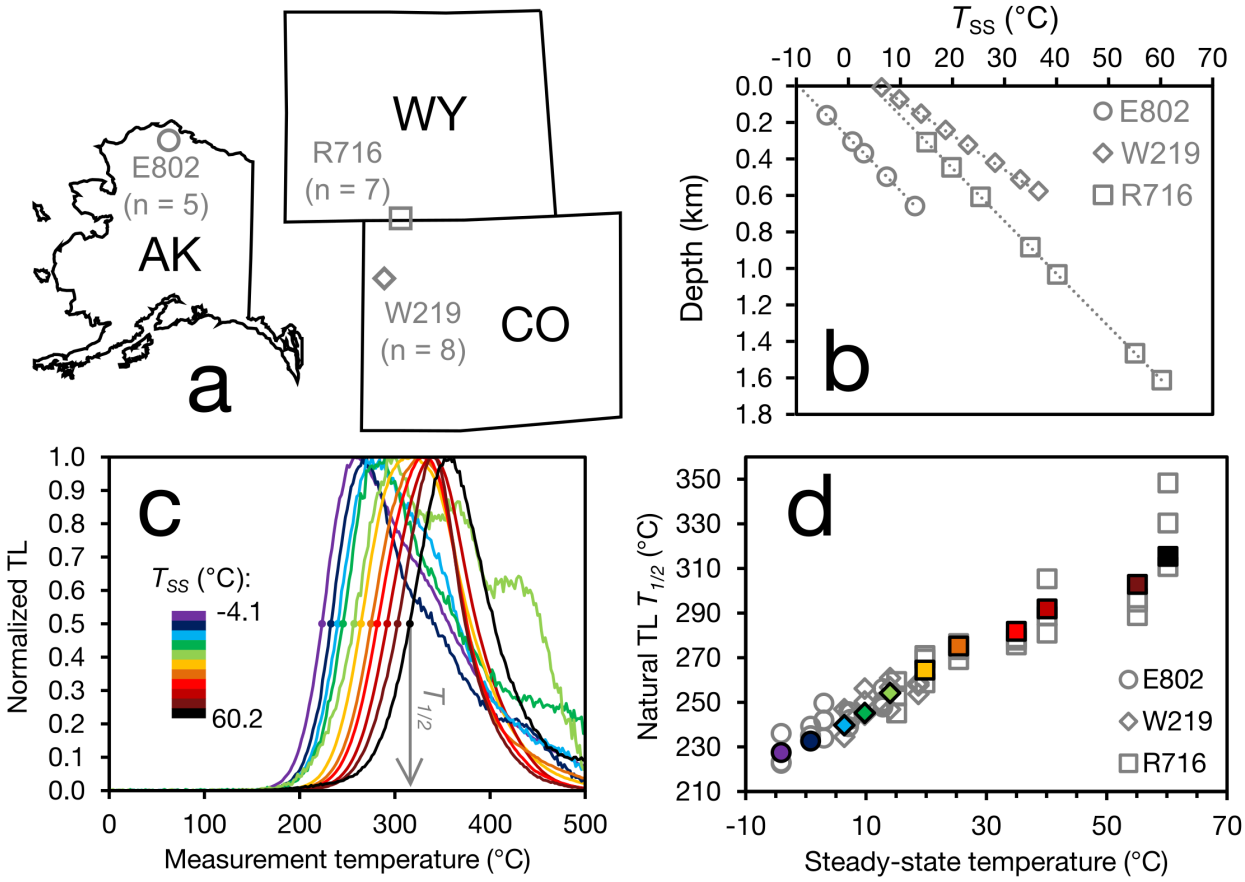

Figure 1: (a) Bedrock sample locations are shown for each of the three USGS CRC drill core sites: E802, W219, and R716. (b) Also shown are the steady-state temperatures for the drill core samples, according to their depths. (c) Representative natural TL signals are colored according to their steady-state temperature, T_{SS}. The $T_{1/2}$ values for these TL curves (normalized to maximum intensity) are shown as solid circles in (c) and are plotted as a function of T_{SS} in (d). The colored symbols in (d) derive from the TL curves shown in (c). The grey symbols represent all of the measured $T_{1/2}$ values, i.e., every aliquots for every sample (see also Fig. 2).

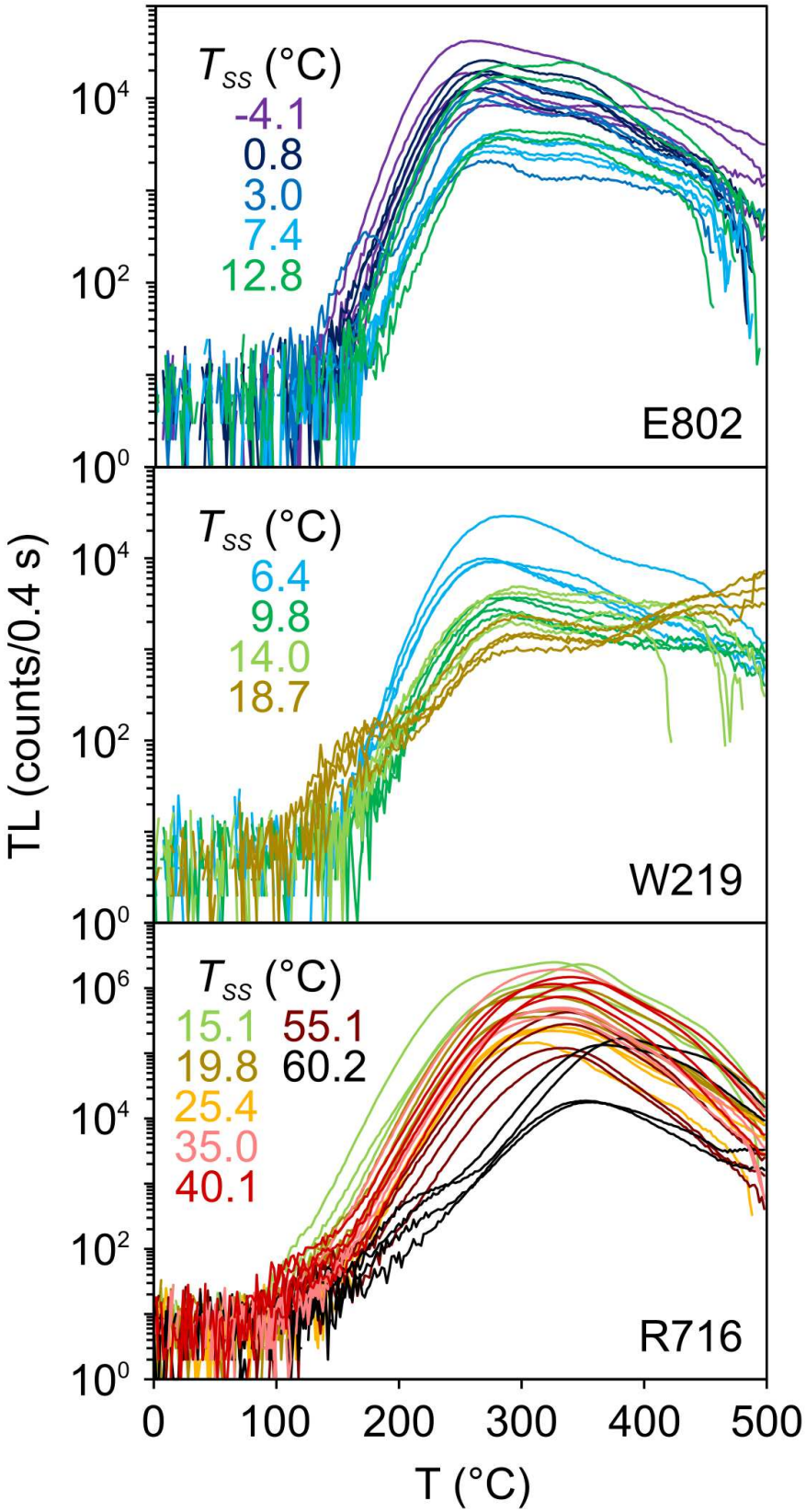

Figure 2: The natural TL signals are plotted by drill core and colored according to the steady-state temperature, T_{SS} (four aliquots are shown per sample). Missing data points within a TL curve signify that the thermal background curve (TL measured after the natural signal and with no dose) at that time bin is larger than the natural signal. Notice the shift in the leading edge and the decreasing brightness as the natural T_{SS} value increases. Notice also the logarithmic y-axes which allow for comparison between the brighter, colder samples and the dimmer samples at higher burial temperatures.

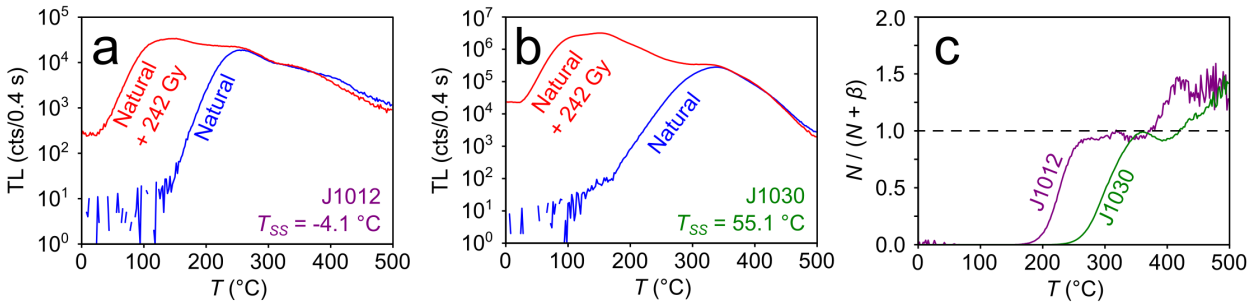

Figure 3: (a) The glow curve shown in blue is a natural aliquot of sample J1012 ($T_{SS} = -4.1$°C; core E802) ($\beta = 5$ °C/s; the thermal background has been subtracted, so some data points are missing). In red is the TL curve of another aliquot of J1012 that has been given a dose of 242.2 Gy in addition to the natural dose. Notice that the low-temperature portion of the TL glow curve grows with dose, whereas no growth occurs above about 250 °C. The same measurements are shown for (b) two aliquots of J1030 ($T_{SS} = 55.1$°C; core R716). (c) The ratios of the natural response to the added-dose response are plotted as a function of measurement temperature for both samples. A ratio of 1 (dashed line) indicates that the sample is in complete field saturation. Notice how the colder sample is nearly saturated (ratio ~ 0.95) at lower measurement temperatures and saturation occurs at higher measurement temperatures for the sample with a higher burial temperature. Above about 375 °C, we see a slight rise in the ratio, which may be attributed to the behavior of a separate, high-temperature peak (Duller, 1997; Murray et al., 2009).

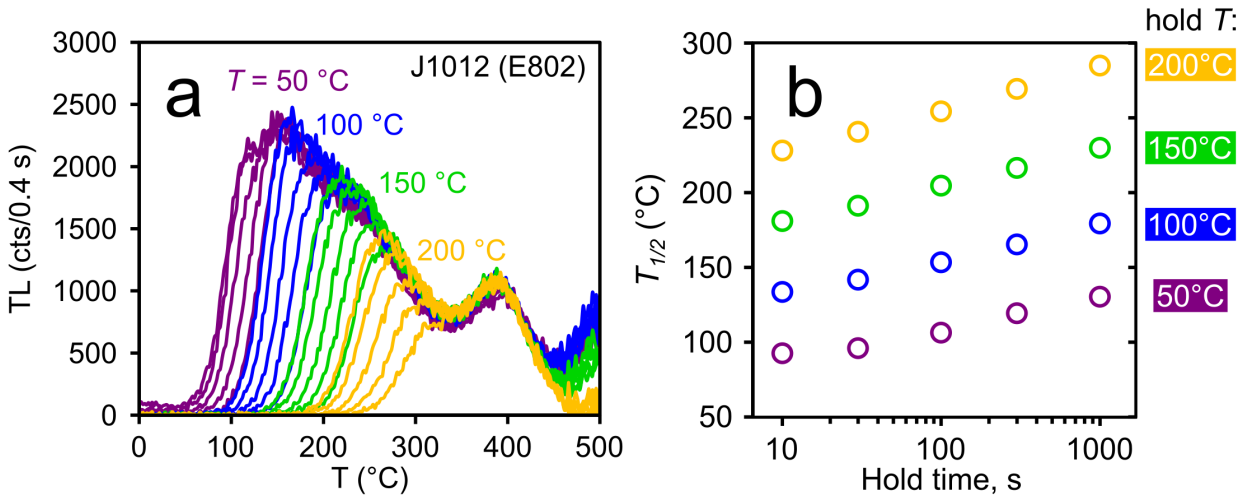

Figure 4: (a) Measured TL curves are shown for sample J1012 (core E802), following isothermal treatments of durations 10, 30, 100, 300, and 1000 s at holding temperatures of 50 (purple curves), 100 (blue), 150 (green), and 200 °C (orange). (b) The $T_{1/2}$ values of these measurements are plotted as a function of hold time and colored according to hold temperature. Notice the shift towards higher $T_{1/2}$ values with longer hold times and higher temperatures.

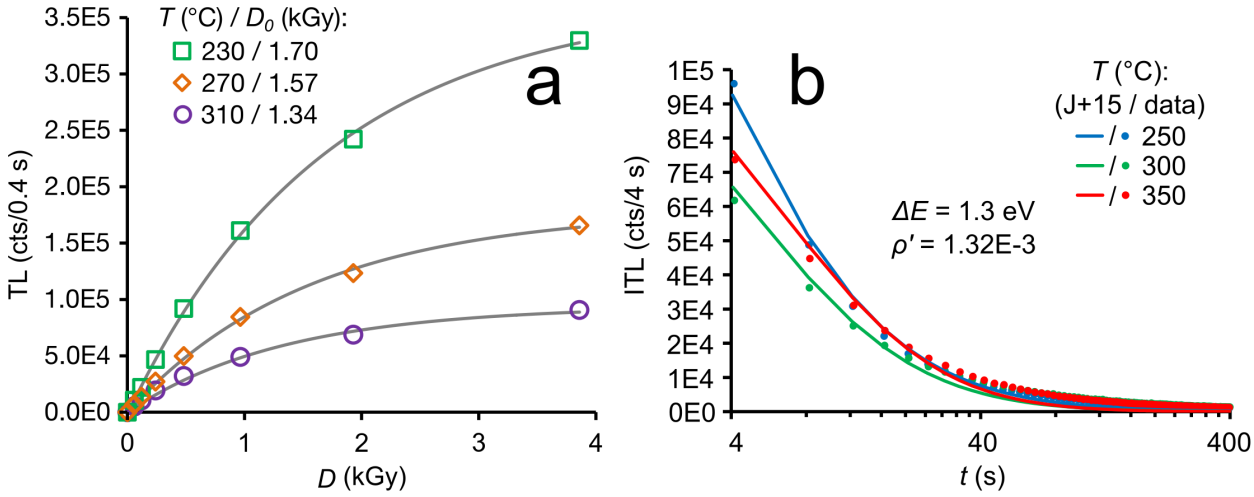

Figure 5: (a) Single-aliquot regenerative (SAR) dose-response measurements of sample J1012 are fitted to a single saturating exponential function. The three TL channels plotted here (230, 270, and 310 °C) represent the observed range of natural $T_{1/2}$ values. The fitted D_0 values at increasing measurement temperatures decrease from 1.70 to 1.34 kGy. (b) The isothermal thermoluminescence (ITL) decay data from sample J1012 following a beta dose of 121 Gy are plotted for a hold time of 400 s at hold temperatures of T = 250, 300, and 350 °C. These decays are fitted to the expression for isothermal decay (Eq. 6) from Jain et al. (2015)('J+15'), using the parameters listed in Table 2 and varying only the initial population (n_0) and the initial lifetime (τ_0) values from one temperature to the next.

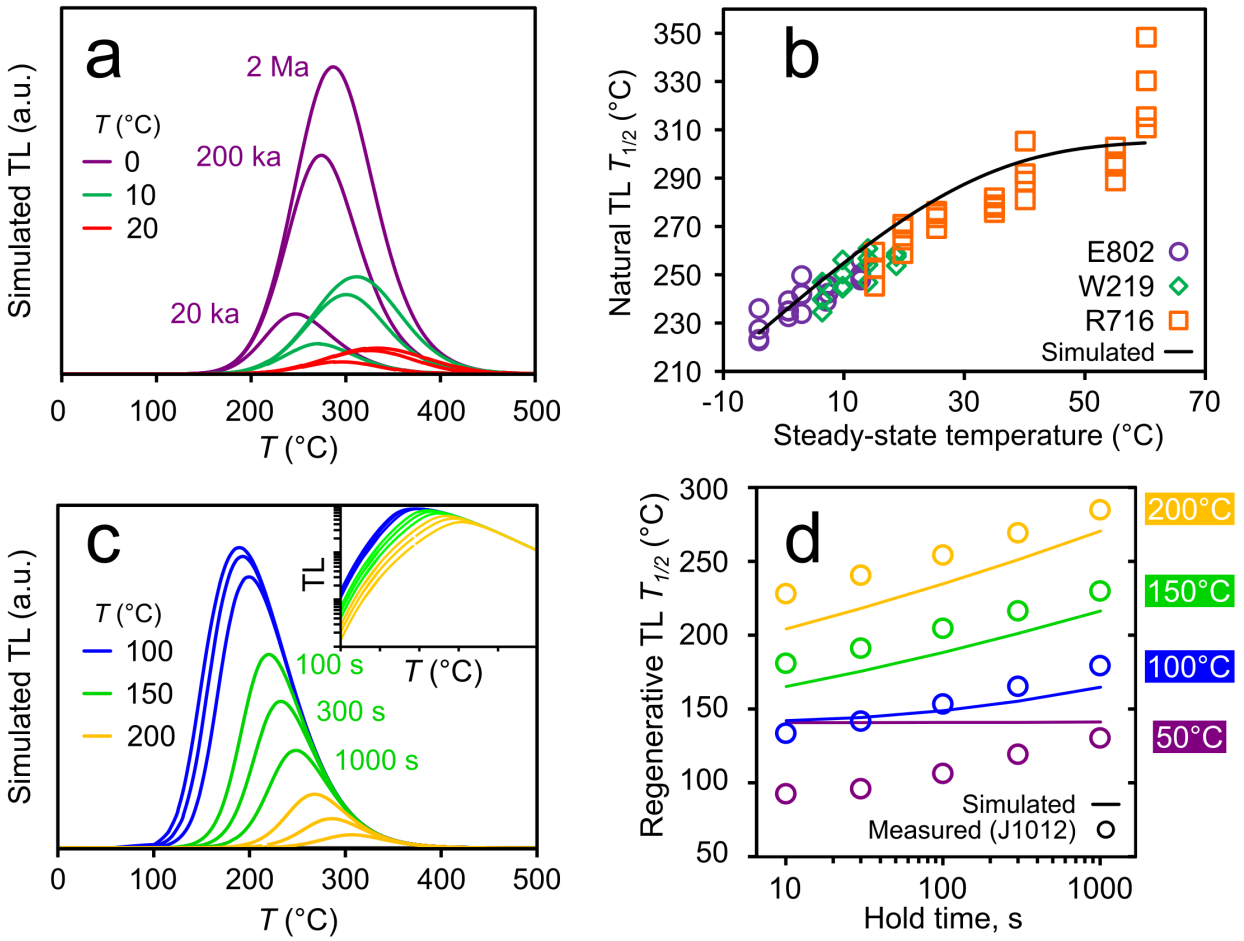

Figure 6: (a) Starting with empty traps, Eq. 1 is solved for isothermal geologic histories. The trapped populations at the final times then become the initial condition for another evaluation of Eq. 1 representing the TL measurement. These are the plotted curves. (Note that after 2 Ma, $n/N \sim 1$ for the most stable traps). (b) This simulation is repeated for each of the steady-state temperature values and the resulting TL $T_{1/2}$ values (solid curve) are compared to the measured $T_{1/2}$ values (open symbols). (c) Instead of reproducing a geologic dose, this experiment reproduces a laboratory dose followed by an isothermal treatment. The simulated TL measurements are shown according to the isothermal conditions. The inset shows a logarithmic y-axis for comparison with Fig. 2. (d) The simulation results from panel (c) are compared against the measured values from sample J1012 (also shown in Fig. 4). For the simulation of geologic and laboratory conditions, the parameters from Table 2 are used.

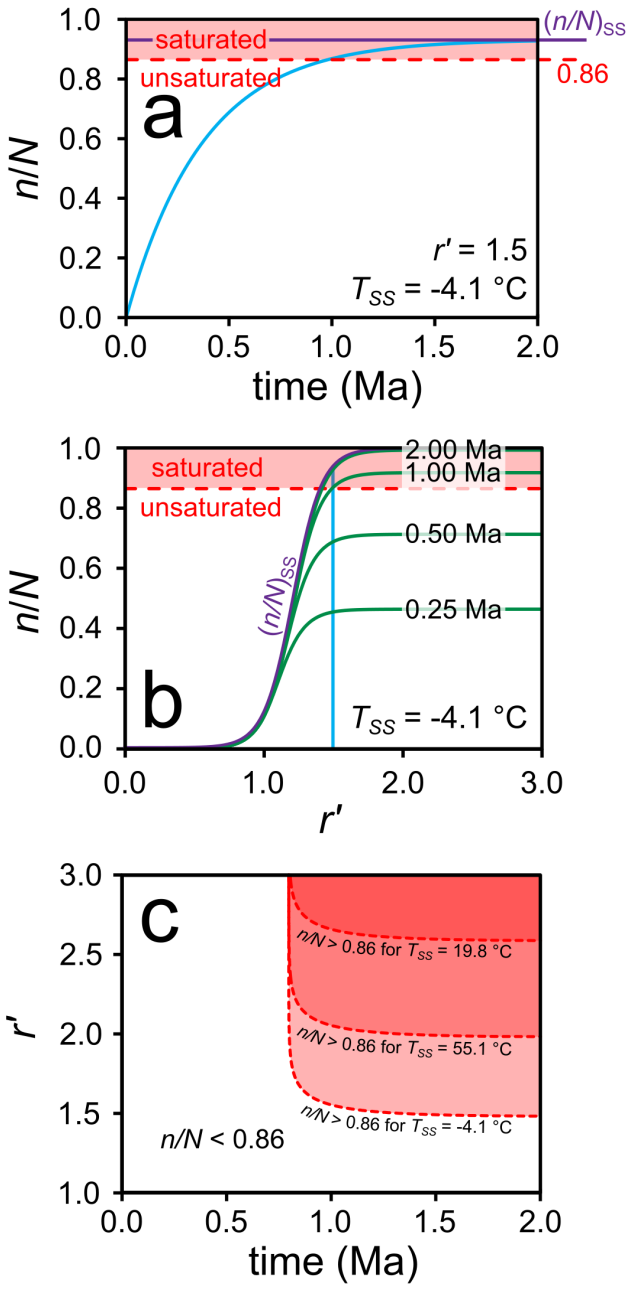

Figure 7: (a) For an arbitrary recombination distance of $r' = 1.5$, trap filling is simulated for 2 Ma at -4.1 °C (T_{SS} for J1012) by assuming an initially empty $n(r')$ distribution that evolves with time according to Eq. 1. After about 1 Ma, the sites at this distance are effectively saturated. Notice that in steady-state at this temperature, not all of the traps will be full, even though they are in steady-state. We illustrate this steady-state limit ($(n/N)_{SS}$) with a purple line. This represents the upper-limit for the concentration of trapped electrons at this temperature. (b) This process is then shown for a range of recombination distances within a lattice, at the same constant temperature ($T = 4.1$ °C). The sites with the greatest recombination distances reach effective saturation ($n/N > 0.86$) first, while those with nearer recombination centers remain unsaturated ($n/N < 0.86$). Importantly, though all distances have reached their steady-state concentration after about 2 Ma, and will not fill any further unless the temperature lowers. (The single distance illustrated in (a) is shown in light blue.) (c) The saturation domain ($n/N > 0.86$) is modeled for three burial temperatures experienced by the drill core samples (the same samples for which MAAD saturation measurements are shown in Fig. 3). Notice that with higher burial temperatures only the trapping sites with high r' values are occupied.